Geochemistry, Geophysics, Geosystems®

AGU ADVANCING EARTH AND SPACE SCIENCE

RESEARCH ARTICLE
10.1029/2022GC010740

Key Points:

- Compositions of the eight most recent Craters of the Moon lava flows elucidate magma evolution in this polygenetic fissure system
- This compositional study revealed the flows were fed by three previously unrecognized magma compositions with distinct petrologic histories
- The magmas were heterogenous, stratified, and culminated in the eruption of increasingly less evolved flows

Supporting Information:

Supporting Information may be found in the online version of this article.

Correspondence to:

J. Chadwick,
chadwickj@cofc.edu

Citation:

Chadwick, J., Chadwick, C., & Kamenov, G. (2023). Compositional evolution of polygenetic fissure volcanic systems: Insights from the latest eruptions at Craters of the Moon Volcanic Field. *Geochemistry, Geophysics, Geosystems*, *24*, e2022GC010740. https://doi.org/10.1029/2022GC010740

Received 12 OCT 2022
Accepted 10 FEB 2023

Author Contributions:

Conceptualization: Claire Chadwick
Formal analysis: Claire Chadwick, George Kamenov
Investigation: George Kamenov
Methodology: Claire Chadwick, George Kamenov
Resources: George Kamenov
Writing – original draft: Claire Chadwick

Compositional Evolution of Polygenetic Fissure Volcanic Systems: Insights From the Latest Eruptions at Craters of the Moon Volcanic Field

John Chadwick[1], Claire Chadwick[1], and George Kamenov[2]

[1]Department of Geology and Environmental Geosciences, College of Charleston, Charleston, SC, USA, [2]Department of Geological Sciences, University of Florida, Gainesville, FL, USA

Abstract The Craters of the Moon (COM) Volcanic Field in Idaho is the largest mostly Holocene lava field in the conterminous U.S. and the site of the most recent volcanism in the Yellowstone-Snake River Plain province. This prominent example of a polygenetic fissure field has produced over 60 eruptions over the past 15,000 years from the Great Rift fissure system. The eight most recent lava flows, known as Period A, were erupted between about 2,500 and 2,000 years ago. In this study, major and trace element and Pb-Sr-Nd isotope data were obtained, with several samples collected from each flow from widely spaced locations to evaluate heterogeneity in their source magmas. The results reveal three previously unrecognized compositional groups that may represent separate magma batches, and that assimilation and fractional crystallization (AFC) controlled the evolution of the entire Period A suite. The three oldest flows were periodic withdrawals from a body of highly evolved and poorly homogenized magma, and four later flows represent successive samplings from a stratified body of more primitive magma. These two flow groups are related via variable AFC modeled with Magma Chamber Simulator software, with Neogene rhyolite as a plausible crustal assimilant. A third compositional type that requires a different parent magma and AFC history is represented by a single flow erupted from vents a few km away from the others. The compositional evolution and variability observed in this sequence of flows provide new insights into how magmas are generated, modified, and delivered in such polygenetic fissure systems.

Plain Language Summary The Craters of the Moon Volcanic Field is a prominent example of a long-lived eruptive fissure system in a continental setting, where lava flows are produced at the Great Rift, a linear zone of fracturing and extending crust on the Snake River Plain in southern Idaho. Craters of the Moon has produced more than 60 eruptions over the past 15,000 years, including young lavas with high-silica compositions that are relatively uncommon in the region. The eight most recent lava flows, known as Period A, were erupted between about 2,500 and 2,000 years ago. This sequence of flows provides snapshots of the evolving system over time and constrains processes that modify and feed magmas to this type of volcanic system. New chemical and isotope data with higher precision than in previous studies reveal that the flows fall into three compositional groups, likely reflecting separate magma batches with distinct histories of cooling, crystallization, and contamination by wall rock. These results illuminate the processes that deliver and alter magmas in such long-lived fissure systems.

1. Introduction

Craters of the Moon (COM) in southern Idaho (Figure 1) is the largest late Pleistocene to Holocene lava field in the conterminous U.S., covering 1,600 km^2 with a total volume of about 30 km^3 (Kuntz et al., 1992). COM is located on the north side of the Eastern Snake River Plain (ESRP), a 300-km-long lowland that is widely perceived to result from the passage of the region over the stationary Yellowstone hotspot during the Neogene (Fouch, 2012; Pierce & Morgan, 1992, 2009). Since then, an extensive suite of post-hotspot lavas has paved the ESRP from widely scattered, mostly monogenetic eruptions (Kuntz et al., 1992; Malde, 1991), but the COM field is notable among the young eruptive centers for its long-lived polygenetic activity. It has produced over 60 eruptions from closely spaced vents along the Great Rift fissure system starting about 15,000 years B.P (Kuntz, Spiker, et al., 1986; Kuntz et al., 1992).

Paleomagnetic data, stratigraphic relations, and radiocarbon dating of charcoal from between some COM flows show that its polygenetic activity has been episodic, with periods of quiescence lasting hundreds to thousands of

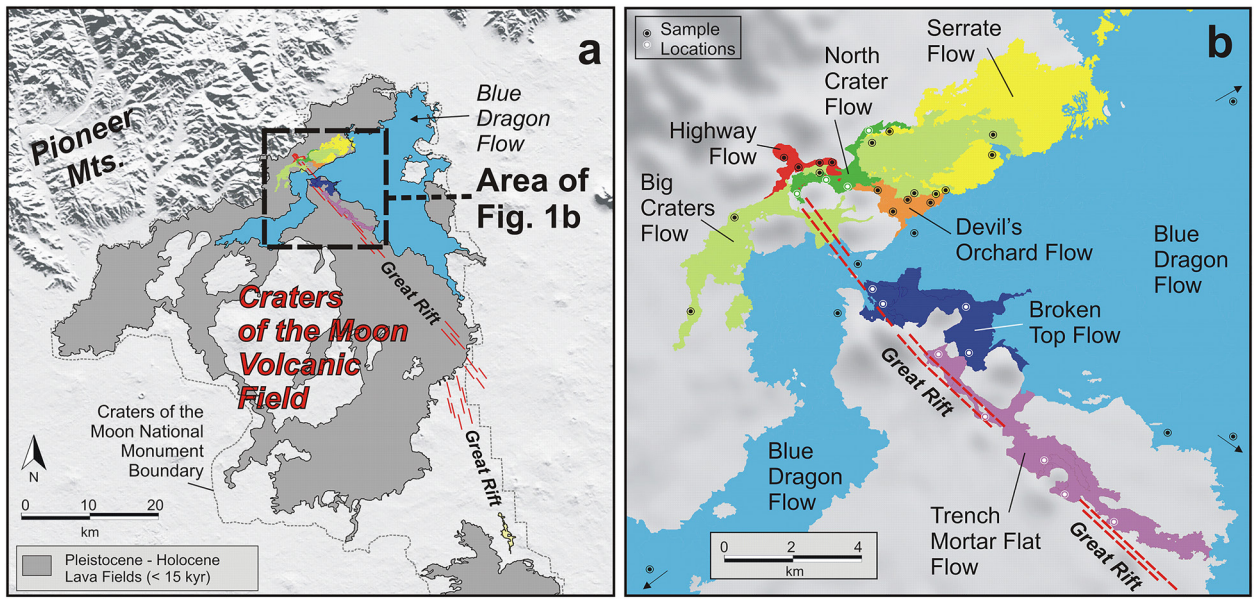

Figure 1. (a): The Craters of the Moon Volcanic Field lies on the north side of the Eastern Snake River Plain along the Great Rift fissure zone and has produced at least 60 flows between about 15,000 and 2,000 years ago. (b): Most of the eight Period A eruptions had sources within a few km of the northern terminus of the Great Rift, with the exception of the Trench Mortar Flat flow that was erupted from fissures 5–7 km further south. Small dots indicate rock sample locations for this study. The colors used to distinguish flows on this map are also used for symbols in graphs in this report. Flow boundaries in panel (b) adapted from Kuntz et al. (1989); GIS mapping data from the National Park Service DataStore: https://www.nps.gov/articles/nps-geodiversity-atlas-craters-of-the-moon-national-monument-preserve-idaho.htm#gri.

years between active eruptive phases (designated Periods A to H) that each produced multiple eruptions (Kuntz et al., 1982; Kuntz, Spiker, et al., 1986). Period A was the most recent active phase, with eight flows emplaced between about 2,500 and 2,000 years ago following a circa 1,000-year hiatus after Period B ended (Kuntz, Spiker, et al., 1986). The Period A flows are informally named in previous works as the Highway, Devil's Orchard, Serrate, Big Craters, North Crater, Trench Mortar Flat, Blue Dragon, and Broken Top flows (Kuntz, Champion, et al., 1986; Kuntz et al., 1988; Stearns, 1928). Many of the conspicuous volcanic features that draw tourists to Craters of the Moon National Monument are exhibited in these young Period A flows.

Previous studies of post-hotspot lavas from across the ESRP show they are mostly primitive olivine tholeiite basalts (Hughes et al., 1999; Kuntz et al., 1992; McCurry et al., 2008), which appear to be minimally modified by fractional crystallization of olivine and plagioclase (Kuntz et al., 1992; Leeman, 1982; Menzies et al., 1984; Stout & Nicholls, 1977). The COM lavas have more diverse and evolved compositions, including comparatively iron-, phosphorus-, and alkali-rich compositions, and ranging from basalts and trachybasalts to trachytes (Kuntz et al., 1985; Kuntz, Champion, et al., 1986; Leeman et al., 1976; Putirka et al., 2009). The COM flows are the youngest of a group of subordinate intermediate and evolved post-hotspot lavas found across the ESRP that were erupted among the more common tholeiites (Ganske & McCurry, 2006; McCurry et al., 2008).

A primary focus of previous COM geochemical studies was to investigate the possible origins of the distinctive lava compositions (e.g., Kuntz et al., 1992; Leeman et al., 1976; Putirka et al., 2009; Stout et al., 1994). COM magmas may be derived from the more common tholeiites but appear to have been further transformed by assimilation and fractional crystallization (AFC) (Kuntz, Champion, et al., 1986; Putirka et al., 2009; Stout et al., 1989), with a more complex suite of fractionating phases including olivine, plagioclase, clinopyroxene, apatite, and magnetite (Menzies et al., 1984; Stout et al., 1989). Potential assimilation candidates include granulites and Neogene, hotspot-related rhyolite, which occur as xenoliths in the most evolved COM flows (Leeman & Manton, 1971; Leeman et al., 1985; Stout et al., 1994). Other potential assimilants include Neogene granitoid plutons (McCurry et al., 2008), Eocene Challis volcanics (Kuntz, Champion, et al., 1986; Norman & Mertzman, 1991), and Archean continental crust (Menzies et al., 1984). A mosaic of cratonic blocks exists beneath the ESRP, and COM lies near sutures between the Archean Grouse Creek block (>2.5 Ga), Paleoproterozoic terranes (2.45–1.6 Ga) and the Cretaceous-Eocene Idaho Batholith (Foster et al., 2006). Putirka et al. (2009) suggested that the local presence

at COM of such low-density crustal rocks could temporarily inhibit the rise of dense mafic magmas, resulting in prolonged storage times and increased AFC compared with elsewhere on the ESRP. Sedimentary rocks found in the neighboring Basin and Range do not appear as xenoliths in any ESRP lavas, suggesting that these lithologies do not underlie large tracts of the volcanic province (Kuntz et al., 1992).

Less attention has been paid at COM to comparatively short-term compositional changes between successive eruptions, which can illuminate shorter-timescale magmatic processes such as fractional crystallization, crustal assimilation, or mixing in this polygenetic system. Given their close relationship in time and space (erupted from within a few km of each other along the Great Rift fissure system), the eight youngest Period A flows may have been supplied by a common shallow magma reservoir and provide successive snapshots of the evolving system over time. In this study, new major and trace element analyses and Pb, Sr, and Nd isotope ratios from the Period A flows are evaluated to assess changes and trends over the series of eruptions. In addition, multiple rock samples were collected from widely separated locations on each flow to evaluate the within-flow compositional variability. The scope of their geochemical variations reflects the heterogeneity of the magma batches that fed them and can illuminate the possible roles of recharge, mixing, or stratification of the source magma.

1.1. Geologic Setting

The COM volcanic field and other young lavas on the ESRP are the most recent products of the Yellowstone-Snake River Plain (YSRP) system, which began with the eruption of the Columbia River flood basalts and subordinate rhyolites about 17 Myr ago in southeast Oregon, northern Nevada, and southwest Idaho (Camp et al., 2013). The NE-trending, time-transgressive Neogene and Quaternary chain of calderas and rhyolite ignimbrites that formed across southern Idaho to the Yellowstone Plateau in northwest Wyoming is widely thought to result from the passage of the North American continent over the fixed Yellowstone hotspot (Coble & Mahood, 2012; Jordan et al., 2004; Nash et al., 2006; Pierce & Morgan, 1992, 2009; Shervais & Hanan, 2008; Smith et al., 2009). In southern Idaho, the midcrust under the ESRP is interpreted to be a MASH-like system of preexisting country rocks and layered mafic intrusions emplaced by the hotspot as the crust passed over it (Braile et al., 1982; Christiansen & McCurry, 2008; Leeman et al., 2009; McCurry & Rogers, 2009; Peng & Humphreys, 1998; Shervais et al., 2006). The prominent topographic depression of the ESRP may result from flexural down warping driven by the dense midcrustal intrusions (McQuarrie & Rodgers, 1998; Rodgers et al., 2002).

As the trace of the hotspot progressed across southern Idaho and created the ESRP, the adjacent Rocky Mountains underwent attendant NE-SW extension, leading to block-faulted Basin and Range mountains uplifted along NW trending normal faults (Anders & Sleep, 1992). The Pioneer Mountains just north of the COM field is one of these ranges (Figure 1). This regional deformation is accommodated on the ESRP by coherent SW motion of the plain and supplemented by internal extension via NW trending belts of fissures and mafic dike intrusions (Chadwick et al., 2007). These fissure systems have fed the mostly mafic Pliocene to Holocene post-hotspot volcanism on the ESRP that flattened its floor and buried older Yellowstone rhyolites to a depth of up to about 1.5 km (Whitehead, 1992). These younger eruptions, including the COM field, have followed no time-transgressive pattern (Hughes et al., 2002; Kuntz et al., 1992; Malde, 1991).

The nature of post-hotspot volcanism on the ESRP suggests it is the type locality for a category of continental activity termed basaltic plains volcanism (Greeley, 1982). Essentially a low-magnitude flood basalt province with relatively lower flow volumes, this activity is characterized by the absence of a large central edifice, with numerous widely emplaced mafic flows and low shields associated with the extensional fissures. The COM field has erupted along the most conspicuous of the ESRP extensional fissure systems, the Great Rift, a 2–8 km-wide belt of noneruptive and eruptive fissures, shields, and cinder and spatter cones, along with extensive lava flows (Kuntz et al., 1982). The Great Rift extends nearly across the width of the ESRP, with COM located on its north side and two other Holocene lava fields, the King's Bowl and Wapi fields, about 60 km to the south. These southern flows erupted during the COM Period A interval (Kings Bowl 2,222 ± 100 years, Wapi 2,270 ± 50 years) and were comprised of olivine basalts typical of the ESRP (Kuntz, Champion, et al., 1986).

COM flows erupted from vents along a 30 km stretch of the northern Great Rift, with the different eruptive periods generally focused along particular sections (Kuntz et al., 1988). The eight Period A flows were sourced from vents on the north end of the rift near its terminus at the Pioneer Mountains (Figure 1). Seven were closely sourced within about 3 km of each other, but the Trench Mortar Flat Flow (the sixth flow in the series) erupted

from several fissures 5–7 km to the south of the others (Kuntz et al., 2007). The Period A lavas all flowed to the east of their source fissures, with the Big Craters and Blue Dragon flows deposited on both the east and west sides. Due to the proximity of their source vents, the earlier flows are partly buried by more recent ones. The first three Period A flows are dominated by block and a'a flow morphologies and were surface-fed. The five younger flows are mostly pahoehoe and were surface-fed or both surface- and tube-fed (Kuntz et al., 2007). The Blue Dragon flow is by far the largest in Period A (280 km^2) and exhibits a complex system of tubes that fed flows over 30 km from their source at the Great Rift (Chadwick et al., 2019; Kuntz, Spiker, et al., 1986).

2. Materials and Methods

2.1. Field Methods

Thirty-nine whole rock samples were collected from the eight Period A flows, with 4–6 samples obtained from the smaller flows and 7 from the larger Blue Dragon Flow. The samples were obtained from widely separated locations on each flow to characterize their compositional variations. Fresh-looking 50–100 g samples were collected with some surface glass attached. Hand-held GPS latitude-longitude locations were obtained for each sample in the WGS 84 datum (Table S1 and Figure 1).

2.2. Major and Trace Elements

Whole rock samples were prepared at the College of Charleston by crushing in a tungsten carbide jaw crusher, and the resulting chips were cleaned in a sonic bath in warm 2 molar Optima HCl for 30 min and rinsed three times in deionized water. Any chips with large phenocrysts or obvious surface contamination were removed, and the remaining chips were finely powdered in an agate ball mill. Glass beads were prepared for X-ray Fluorescence (XRF) analysis by mixing the powders with desiccator-dried lithium tetraborate flux in a 2:1 weight ratio and fused at 1000°C in graphite crucibles for 10 min, cooled, reground to powder, and remelted at 1000°C for 10 more min to make the final beads. For inductively coupled plasma mass spectrometer (ICP-MS) analyses, flux and rock powder were mixed in a 1:1 ratio and the beads were fused at 1000°C for 10 min and cooled. Beads for U.S.G.S. standard BCR-2 were also prepared. Loss on ignition (LOI) was determined by heating aliquots of sample powders to 800°C for 4 hr. Many LOI values were slightly negative, presumably due to oxidation of the relatively high Fe (Rhodes & Vollinger, 2004) and low volatile contents in the rocks (Putirka et al., 2009).

The beads were analyzed at Washington State University GeoAnalytical Laboratory for 29 major and trace elements via XRF and 27 trace elements by ICP-MS. Deviations between measured and accepted values for BCR-2 standard major elements (Raczek et al., 2001) were less than 2%, and for trace elements measured by XRF and ICP-MS were less than 5% and/or less than 1 ppm.

2.3. MELTS and Magma Chamber Simulator AFC Modeling

The potential effects of fractional crystallization in the Period A lava sequence were modeled using MELTS software (rhyoliteMELTS 1.2.0, Gualda et al., 2012). A family of liquid lines of descent (LLD) was modeled using the most mafic sample measured in the study as the starting composition. A range of pressures, water contents, and oxygen fugacity buffers were used to model LLD curves that would best match trends in the Period A major element data. To further assess the potential effects of fractional crystallization combined with wall rock assimilation, Magma Chamber Simulator (MCS) tools were used. MCS uses the suite of MELTS engines to numerically quantify magma evolution with computations run in an Excel worksheet (Bohrson et al., 2020; Heinonen et al., 2020). The software calculates magma evolution in two stages: the MCS-PhaseEQ tool calculates major element evolution, and MCS-Traces uses the MCS-PhaseEQ output to model trace element and radiogenic isotope evolution. The initial magma and wall rock compositions used in the modeling were literature data for primitive COM samples and local rhyolites or xenoliths, respectively. A range of input parameters were tested including the initial magma and wall rock temperatures, system pressure, water content, and mineral/melt partition coefficients collected from the GERM database (https://kdd.earthref.org/KdD/) for minerals predicted by MCS-PhaseEQ to be in the magma and wall rock.

2.4. Radiogenic Isotope Methods

For Pb, Sr, and Nd isotopic analyses, 0.05 g of the cleaned whole rock chips was dissolved in Teflon vials in Optima grade concentrated HF and HNO_3 acids and dried down, and the residue was dissolved in Optima-grade HCl and dried down. Pb, Sr, and Nd were extracted from the residue using a series of ion exchange columns. The

samples were first centrifuged and passed through 100 µl of 100–200 mesh Dowex 1X-8 resin, with the Sr and Nd fractions collected in 3 ml of 1N HBr acid. Then, 1 ml of Optima 20% HNO_3 was flushed to collect the Pb fraction, and these were evaporated to dryness for Pb isotope analysis. The Sr and Nd cuts were dried down and then dissolved in 3.5N HCl, centrifuged, and passed through AG50W-X12 200–400 mesh resin. A total of 17 ml of 3.5N Optima HCl was flushed, and the Sr fraction was collected in 5 ml of 3.5N HCl and dried. Two ml of 6N HCl was then washed and the Nd fraction was collected in 12 ml of 6N HCl and dried. The Sr fraction was dissolved in HNO_3 and purified by passing through 100 µl Sr-Spec resin, with a total of 1.4 ml 1N HNO_3 washed and Sr collected in 1.5 ml of 18 megaohm distilled water and dried down for analysis. The Nd fraction was then passed through Ln-spec resin, with a total of 7 ml of 0.25N HCl flushed and Nd collected in 4 ml of 0.25N HCl and dried down for analysis.

The Pb, Sr, and Nd isotopic ratios were measured at the University of Florida Department of Geological Sciences using a Nu-Plasma multiple-collector ICP-MS (MC-ICP-MS) following methods described in Kamenov et al. (2007). In short, all isotopic ratios were measured in static mode. The $^{87}Sr/^{86}Sr$ ratio was corrected for mass-bias using exponential law and $^{86}Sr/^{88}Sr = 0.1194$. Nd isotope measurements were corrected for mass-bias using $^{146}Nd/^{144}Nd = 0.7219$. Pb isotope analyses were conducted using the Tl normalization technique (Kamenov et al., 2004). The reported isotopic ratios are relative to the following long-term standard values: NBS 987 $^{87}Sr/^{86}Sr = 0.71024$ (± 0.00003, 2σ), JNdi-1 $^{143}Nd/^{144}Nd = 0.512115$ (± 0.000021, 2σ), and NBS 981 $^{206}Pb/^{204}Pb = 16.937$ (± 0.004, 2σ), $^{207}Pb/^{204}Pb = 15.490$ (± 0.003, 2σ), and $^{208}Pb/^{204}Pb = 36.695$ (± 0.009, 2σ).

3. Results

3.1. Major Elements

The new whole-rock major element data for the eight Period A flows are listed in Table S1 and displayed in Figures 2–4. Raw major element totals for samples and standards ranged from 98.3% to 99.8%, and the totals in Table S1 are normalized to 100%. The data define generally coherent trends in Harker diagrams (Figure 2), with samples from the oldest three flows (Highway, Devil's Orchard, and Serrate) exhibiting the highest SiO_2, Al_2O_3, Na_2O, and K_2O and the lowest MgO, FeO* (FeO as total iron), P_2O_5, TiO_2, and CaO. The five later flows have more mafic and less evolved compositions. Samples from the Trench Mortar Flat Flow have subtle aberrations from the coherent trends for some major elements, including lower values of FeO and Na_2O and higher MgO and TiO_2 than the other younger flows for a given SiO_2 (violet symbols in Figure 2). On a TAS diagram (total alkalis vs. silica; Figure 3), the Period A flows trend across the high-alkali trachybasalt, basaltic trachyandesite, trachyandesite, and trachyte fields (Kuntz et al., 1992). Their wt. % K_2O is more than 2% higher than Na_2O, thus they can be classified as potassic trachybasalts, shoshonites, latites, and trachytes (Le Bas et al., 1986). The lavas are higher in FeO, Na_2O, P_2O_5, K_2O, and TiO_2 and lower in MgO, Al_2O_3, and CaO than typical ESRP tholeiites at a given SiO_2 (Hughes et al., 2018; Kuntz et al., 1985; Putirka et al., 2009).

The major element data show two time-variant trends in the Period A sequence (Figure 4). First, the flows form two broad compositional groups; the three oldest flows have the highest intraflow variability, with basaltic trachyandesites, trachyandesites, and trachytes sampled from different parts of individual flows (e.g., SiO_2 varies by >11% in Serrate Flow samples). Apparent compositional gaps between data points for these older flows are likely due to their broad variability combined with a sampling bias, with significant portions of the flows inaccessible due to their burial by the younger flows and sampling difficulties due to the remoteness and rugged terrain. The later five flows have more restricted compositions but still have intraflow variations (e.g., SiO_2 varies by ~2%–5%). The compositional ranges for the silica-rich early flows and more mafic later flows overlap, with one sample each from the Devil's Orchard and Serrate flows (and one literature sample from the Serrate flow, Putirka et al., 2009) that are very similar to the Big Craters flow for all major elements (Figures 2–4).

The second time-variant trend observed in Period A is a broad progression over the series to more primitive compositions, with declines in the average and lowest measured values (including literature data) of SiO_2, Al_2O_3, K_2O, and Na_2O and concomitant increases in TiO_2, FeO, MgO, CaO, and P_2O_5 with each succeeding eruption (Figure 4). These trends culminate with the lowest SiO_2 and highest MgO in Period A measured in a sample from the last-erupted Broken Top flow.

The major element trends in Period A are broadly consistent with the expected effects of fractional crystallization of the mineral phases observed in thin section (olivine, plagioclase, clinopyroxene, apatite, magnetite), albeit with the most evolved lavas erupted first in the series followed by more primitive compositions. MELTS software

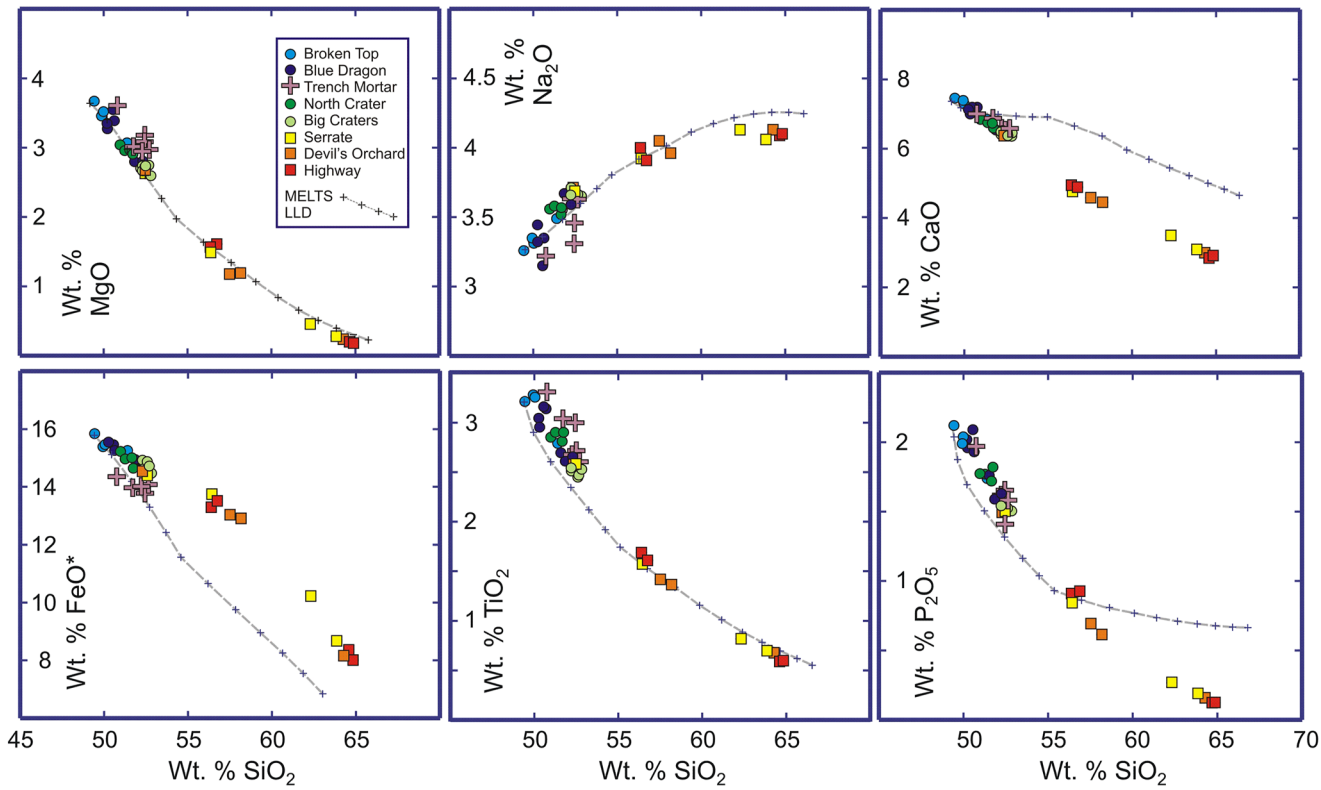

Figure 2. Major elements for samples from the eight Period A lava flows form generally coherent trends that are relatively time-dependent, with decreases in SiO_2, Al_2O_3, Na_2O, and K_2O, and increases in MgO, TiO_2, CaO, FeO*, and P_2O_5 over the eruptive sequence. These trends correspond with observed mineral phases and fractionating phases predicted by MELTS given the most mafic sample (BT-3 from the Broken Top flow) as the starting composition, suggesting an important role for fractional crystallization in their evolution. However, MELTS runs with a variety of pressures, water contents, and oxygen fugacity buffers did not produce liquid line of descent (LLD) trends that fit all major elements, indicating a possible role for wall rock assimilation (the LLD shown is the one that best conforms to the MgO data—pressure 3,000 bars, 1.5% H_2O, -2FMQ fO_2 buffer). The Trench Mortar Flat Flow (violet symbols) has slightly lower FeO and Na_2O and higher MgO and TiO_2 than the other younger flows for a given SiO_2.

modeling produced a family of LLD using the most mafic sample from the Broken Top flow (BT-3) as the liquid parent, with a range of pressures from 1,000 to 4,000 bars (100–400 MPa), H_2O contents (0%–1.5%), and oxygen fugacity buffers (−0.5 to −2 QFM). MELTS correctly predicted the observed phenocryst minerals (if whitlockite formation was suppressed), and various LLD closely followed the trends for some major elements, but none were generated that matched the trends for all elements (Figure 2).

3.2. Trace Element Results

The trace element data show more clearly that the Period A lavas can be split into three distinct compositional groups: (a) the more enriched and diverse first three flows (Highway, Devil's Orchard, and Serrate), (b) four later, less enriched and less heterogenous flows (Big Craters, North Crater, Blue Dragon, and Broken Top), and (c) the anomalous Trench Mortar Flat Flow.

Some trace elements form trends that closely correspond with major element variation for all Period A flows, with relatively correlated increases in Ba, Nb, Pb, U, and Rb and decreases in Sr (Figure 5a) with increasing SiO_2. For others such as the rare earths (REE), Hf and Zr, plots show scatter or declines in their concentrations as SiO_2 increases (Figure 5b), especially for the three more enriched early flows. The later, lower-silica group shows gradual, subtle decreases in incompatible trace element enrichment with each successive eruption that follow their major element trends to more mafic values (Figures 5c and 5d). The broader range of trace element variability for the older group overlaps with the younger group as they do for the major elements, with a few samples from the Devil's Orchard and Serrate Flows similar to the subsequent Big Craters Flow. For the Trench

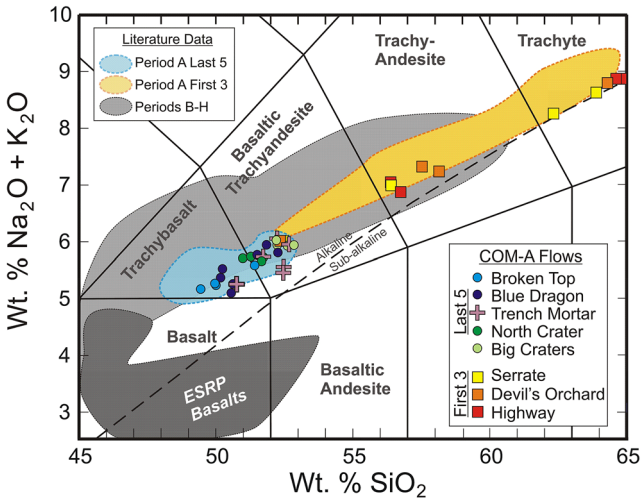

Figure 3. Total alkalis-silica classification diagram after Le Maitre et al. (2002). The first three lavas erupted in Period A exhibit the highest silica and alkali contents at Craters of the Moon (COM), with samples ranging from basaltic trachyandesite to trachyte. Their broad variability slightly overlaps with the more constrained and mafic compositions of the last five flows. The alkaline/subalkaline division line is from Irvine and Baragar (1971). Craters of the Moon literature data (blue and orange fields) from Leeman et al. (1976), Kuntz et al. (1985), Putirka et al. (2009), and Chadwick et al. (2019). Eastern Snake River Plain tholeiite basalt data (dark gray field) from Kuntz et al. (1985), Putirka et al. (2009), and Hughes et al. (2018).

Mortar Flat flow, many trace elements show clear departures from the Period A trends, including higher Ni and lower REE, Ta, Sc, and Y for a given SiO_2 (Figure 5b).

A multielement (spider) plot of trace elements (Figure 6) shows samples from the three early flows to be more enriched in most trace elements than the later flows, with the exceptions of Sr, P, and Ti, which have the deepest depletions in these lavas, indicating more plagioclase, apatite, and magnetite fractionation. Trench Mortar Flat samples (violet curves in Figure 6) are similar to the other young flows for the less incompatible elements but are notably the most depleted in Period A for the REE and Y.

3.3. Isotope Results

The new radiogenic isotope data are consistent with previous work on the COM volcanic field (Leeman & Manton, 1971; Putirka et al., 2009) and better characterize the variability and relationships among the Period A flows. COM $^{87}Sr/^{86}Sr$ versus $^{143}Nd/^{144}Nd$ data (Figure 7a) form a linear array that deviates sharply from the trend for regional SRP tholeiites (Hanan et al., 2008; Jean et al., 2014; Menzies et al., 1984). Lead isotope data for COM form trends that lie just adjacent to ranges of variability for the ESRP (Figure 7b). Period A samples have among the most radiogenic Sr and most unradiogenic Nd and Pb isotopes among all COM lavas (Figures 7a and 7b).

Isotopes for most Period A samples exhibit trends and variability that correlate with their major and trace elements, and generally conform to their place in the eruptive sequence. The three early flows have the most unradiogenic Nd and Pb and most radiogenic Sr ratios, and the later flows trend to higher Nd and Pb and lower Sr (Figures 7a and 7b). The three early flows also have the largest within-flow isotopic variability (e.g., $^{206}Pb/^{204}Pb$ for Serrate Flow samples vary from 17.798 to 17.901), reflecting their major and trace element ranges. The broad compositional variations of the Serrate and Devil's Orchard flows overlap with the younger Big Craters Flow, also reflecting their major and trace element behavior.

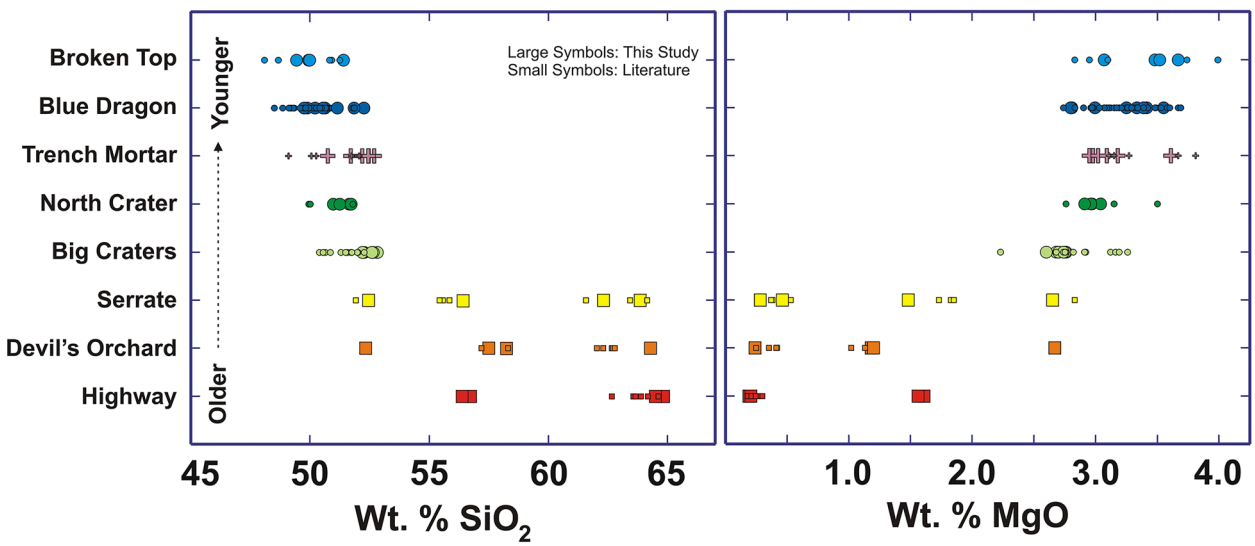

Figure 4. The first three eruptions in the Period A sequence are the most evolved and have the most within-flow diversity. Samples from the five later eruptions are less heterogenous and show a general trend toward more mafic and primitive compositions with eruptive order. The average and lowest-measured SiO_2 composition (new and literature data) progressively decrease and the average and highest-measured MgO composition increase through the series, with the exception of the Trench Mortar Flat flow that shows subtle deviations from the trends for some elements. Data shown are from this study (large symbols) and Leeman et al. (1976), Kuntz et al. (1985), Putirka et al. (2009), and Chadwick et al. (2019) (small symbols).

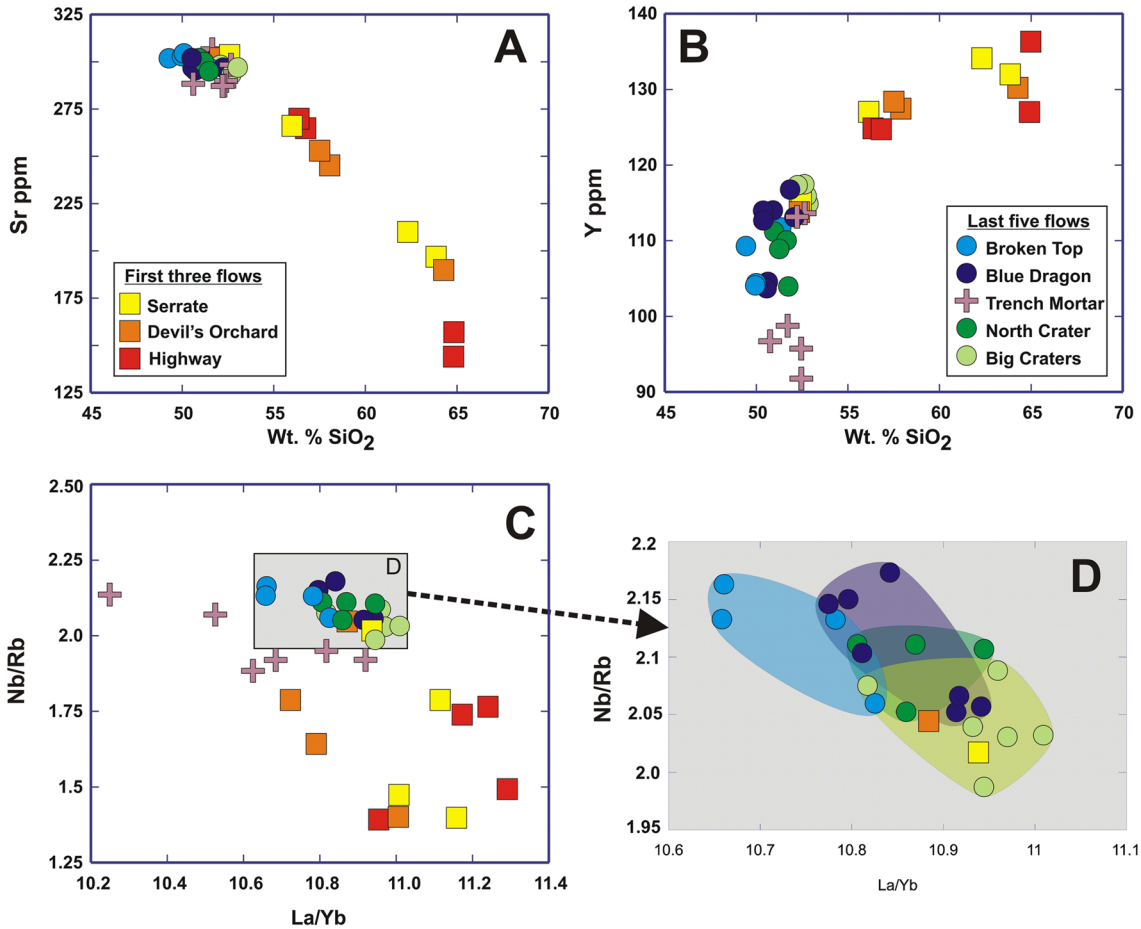

Figure 5. (a) Some trace elements (e.g., Sr) are largely correlated with SiO_2 for the entire Period A suite, (b) but others (e.g., Y) show more scatter for the high-silica, early erupted flows (warm color symbols), as well as divergent trends for the Trench Mortar Flat flow (violet symbols). (c) Trace element ratios also show broad variability among the first three high-silica flows and distinct trends for the Trench Mortar Flat and four other younger, low-silica flows. (d) The Big Craters, North Crater, Blue Dragon, and Broken Top flows have similar trace element characteristics but exhibit weak and overlapping trends related to their eruptive order. The Big Craters Flow (light green symbols) has the highest La/Yb and lowest Nb/Rb in the group, and there is a general decrease in incompatible element enrichment with each successive eruption, with the Broken Top flow (light blue symbols) the last to erupt. The most depleted samples from the Serrate and Devil's Orchard Flows (second and third to erupt, orange, and yellow symbols) overlap with the Big Craters Flow (fourth to erupt), just as they do for the major elements.

Although the Big Craters, North Crater, Blue Dragon, and Broken Top flows have similar isotopic compositions and overlapping ranges, their average values progressively change with each eruption, reflecting the subtle evolution to more mafic and depleted compositions observed in their major and trace elements (Figure 7c). The isotopic variability for the younger flows correlates with their major and trace element variability, with lower interflow heterogeneity than the older group, but the Trench Mortar Flat Flow has higher isotopic variability relative to its major and trace elements. The Trench Mortar Flat also deviates from the temporal trends of the other flows, including the highest Pb and Nd and lowest Sr isotopic ratios of Period A, despite the flow's intermediate composition and place in the eruptive order (Figures 7a and 7b). Although Trench Mortar Flat isotopes are correlated with major elements, they follow divergent paths from the other flows in element-isotope diagrams (Figure 8).

4. Discussion

The results of this study show that the Period A flows provide a window into the evolving magma system over time, revealing its variable heterogeneity and changes that occurred between eruptions. Kuntz, Champion et al. (1986) suggested separating all COM lavas into two categories: a "Contaminated" higher-silica type (that includes the first three Period A flows) with petrographic evidence of assimilation, and a "Fractionated" lower-silica type

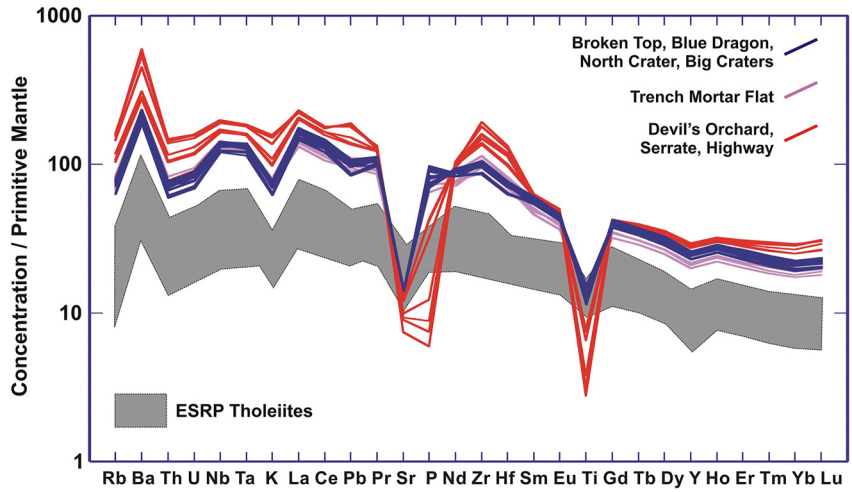

Figure 6. The first three Period A flows (red curves) are more enriched in most trace elements relative to the later five flows (blue curves), except for deeper Sr, P, and Ti depletions. Trench Mortar Flat samples (violet curves) mimic the trace element compositions of the other younger flows for lighter trace elements but are notably less enriched in the REE and Y. Data for the Eastern Snake River Plain tholeiites are from the Kimama drill core (Potter et al., 2018). Primitive mantle composition from Sun and McDonough (1989).

(that includes the last five Period A flows) with no evidence of assimilation and chemical variations that are mainly accounted for by crystal fractionation. The new geochemical data in this study show that all Period A lavas exhibit variations in isotopic ratios that correlate with major and trace elements, consistent with AFC controlling the compositions of the entire Period A suite. Moreover, the variability observed in the Period A flows shows that they can be separated into three compositional and temporal groups that followed separate evolutionary paths. The first includes the earliest three eruptions (Highway, Devil's Orchard, and Serrate) that are dominated by block and a'a flow morphologies, with the most evolved and heterogenous compositions. The second group includes four later flows (Big Craters, North Crater, Blue Dragon, and Broken Top, the fourth, fifth, seventh, and eighth flows, respectively) that are mostly pahoehoe and are more primitive and depleted and have less interflow variability. Finally, the sixth-erupting Trench Mortar Flat Flow is also mostly pahoehoe and has compositional characteristics that are distinct from these two groups and constitutes a third category.

The comparable broad compositional ranges for the first three flows point to their sequential derivation from the same magma batch. Though their source vents are buried by the younger flows, mapping by Kuntz et al. (2007) showed they erupted from the same or closely spaced fissures near the north end of the Great Rift, and it is plausible that they erupted from the same conduit. Their considerable heterogeneity shows that the source magma was poorly homogenized during their eruptions. This may be due to a stratified magma body, with less dense, higher-silica liquids residing at shallower depths and erupting first, followed by increasingly denser and less evolved magmas from deeper in the system. Such a density gradient may have inhibited homogenization over time, and their similar compositional ranges suggest that such stratification remained a stable feature as these first flows erupted.

The second, more primitive and less heterogenous group of four flows (Big Craters, North Crater, Blue Dragon, and Broken Top) shows subtle progressive trends to increasingly mafic and depleted average compositions with each sequential eruption (Figures 4, 5, and 7b), culminating with the most primitive lava in the last-erupted Broken Top Flow. These flows all came from colinear vents near those of the earlier flows, along a 3 km stretch of the Great Rift (Kuntz et al., 2007). Given their similar compositions, clear evolutionary relationship, and proximity of their eruptive sources, they are likely successive samplings from the same dike system and magma storage.

The flows in this second group are more homogenous, but the broad sampling strategy in this study revealed compositional diversity that may again reflect a stratified magma source. Such stratification was proposed by Chadwick et al. (2019) to explain the compositional range in samples from the Blue Dragon Flow and the increasingly mafic lavas that were emplaced during the course of its eruption. This largest Period A flow has surface glass color variations and stratigraphic relations among flow lobes across its surface that allowed for the

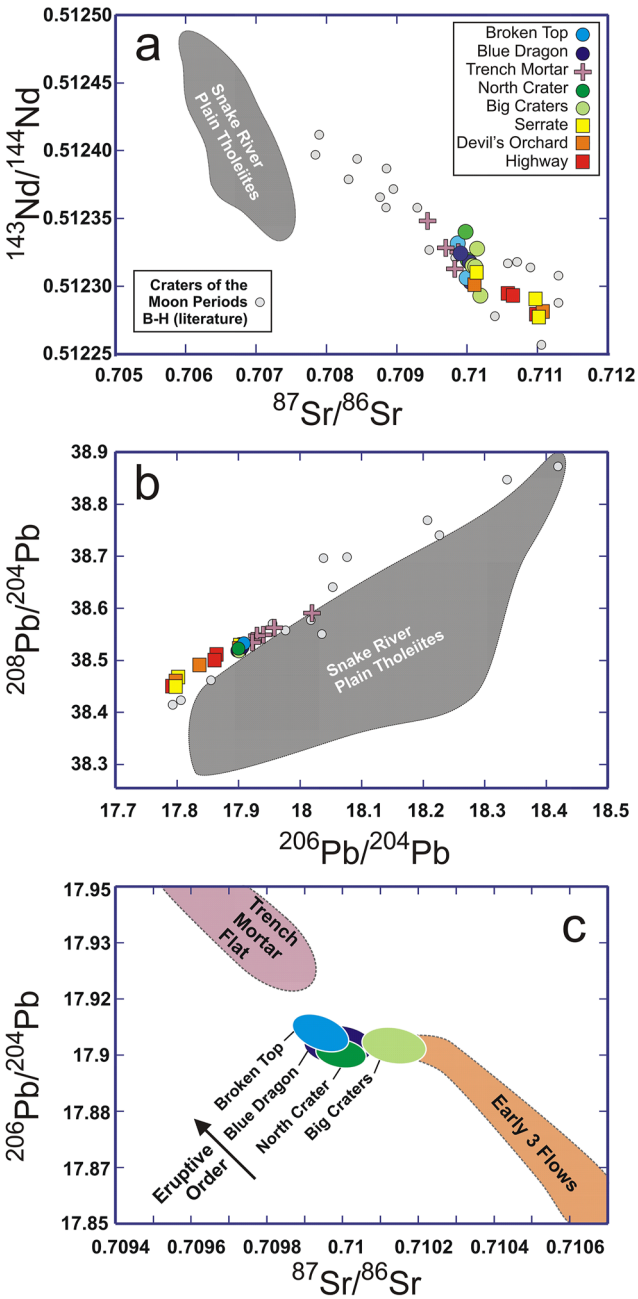

Figure 7. (a) The Sr versus Nd isotope array for Craters of the Moon (COM) diverges from the trend of SRP tholeiites, and samples from the first three Period A flows have among the most radiogenic Sr and unradiogenic Nd values for COM. Trench Mortar Flat (violet symbols) isotopic variability extends to values typical of many older COM eruptive phases (gray dots, literature data) for all radiogenic isotopes measured. (b) Pb isotopic ratios for COM lavas trend along the periphery of data fields for the Eastern Snake River Plain, and Period A samples have among the lowest values for COM. (c) Most of the Period A Pb isotope diversity lies in the three early flows and the Trench Mortar Flat flow, but there are subtle progressive changes in the other young flows that correlate with their eruption order. COM literature data from Putirka et al. (2009) and SRP literature data from Hanan et al. (2008) and Jean et al. (2014).

interpretation of its emplacement history, which revealed that higher silica lavas were erupted first, followed by progressively more mafic lavas from deeper in the system as the flow was emplaced. A stratified magma supply may explain the variable compositions within each flow as well as the gradual changes in composition observed over the whole Period A series, as they may have gradually tapped deeper, progressively more mafic and primitive compositions with each successive eruption. Kuntz, Champion et al. (1986) noted a general trend of earlier, higher silica flows to later, lower silica flows for most COM eruptive periods and proposed vertically zoned magma sources as the most likely explanation.

Although the major and trace element and isotopic compositions of the first and second groups of flows are very different, they define coherent compositional trends that suggest a genetic relationship. The covariation of isotopes with major and trace elements observed in both groups (Figure 8) is characteristic of coupled AFC (DePaolo, 1981; Menzies et al., 1984). Putirka et al. (2009) proposed a two-stage AFC model to transform the prevalent ESRP tholeiitic magmas into the more evolved COM lavas. For the first stage (AFC-1), they envisioned 1% assimilation of a hypothetical deep crustal gabbroic wall rock that would increase $^{87}Sr/^{86}Sr$ without a significant increase in SiO_2, resulting in the formation of the most primitive lavas erupted at COM (Figure 8). These magmas then underwent varying magnitudes of a second assimilation (AFC-2) in their scenario, leading to the variety of more evolved COM compositions.

A series of AFC calculations using MCS software was run to assess the viability of this second phase of AFC in light of the new Period A compositional data (Figure 8). Primitive COM samples from previous eruptive periods were used as the initial magmas for the modeling (Putirka et al., 2009). A variety of potential wallrock assimilants have been proposed to account for COM compositions, including granulites found as xenoliths in some COM flows (Leeman et al., 1985), Eocene Challis volcanics (Kuntz, Champion, et al., 1986), and basement rocks (Menzies et al., 1984). To account for the observed isotopic trends (Figure 7), the crustal assimilant for COM magmas must have more radiogenic Sr and less radiogenic Nd and Pb ratios than the most primitive COM lavas. Putirka et al. (2009) evaluated rhyolitic xenoliths found in COM lavas, presumably derived from a shallow crustal layer of Neogene rhyolite deposited by the Yellowstone hotspot. These were also used in the MCS AFC computations in this study, as well as local rhyolites erupted from the Picabo caldera system at 10.4–6.6 Ma when the Yellowstone hotspot resided beneath the present location of COM (Drew, 2013).

The MCS calculations were performed with a range of conditions, including system pressures, magma and wallrock water contents and initial temperatures, and wallrock to magma mass ratios. The parameters that resulted in evolutionary trends that best matched those in Period A data (Figure 8) were magma and wallrock water content 0.5% and 1%, respectively, system pressure 1,000 bars (100 MPa), whitlockite was excluded from fractionating phases, a 1:1 wallrock mass to magma mass ratio, a wallrock critical melt fraction of 0.4, and a starting magma temperature of 1300°C. An initial wallrock temperature of 670°C was used, consistent with relatively warmer country rocks due to repeated intrusions prior to and during the Period A eruptions. For trace element and isotope modeling in MCS-Traces, mineral/melt partition coefficients were collected from the GERM database (https://kdd.earthref.org/KdD/) for minerals predicted by MCS-PhaseEQ to be present in the magma and wall rock. The iron oxidation state was not known,

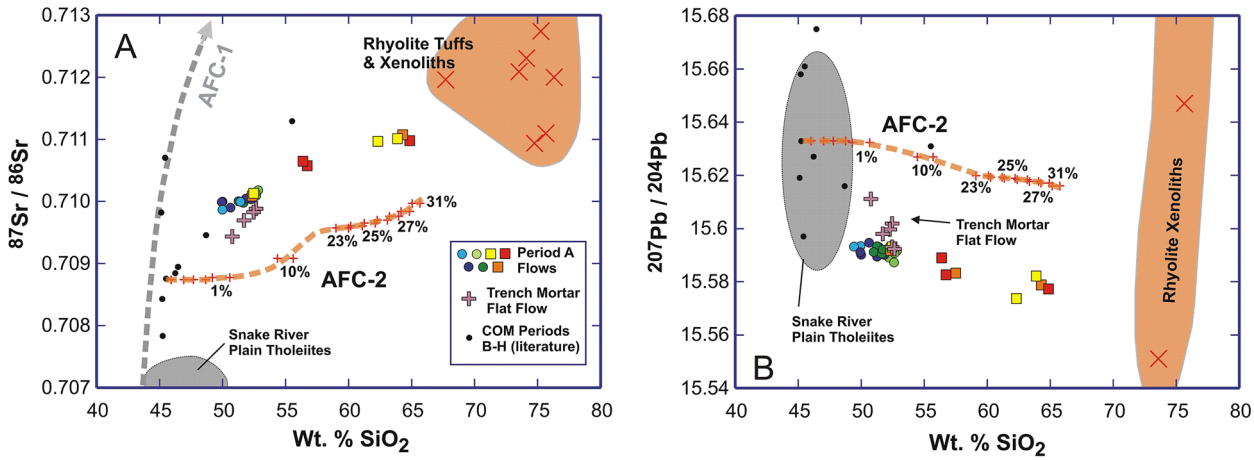

Figure 8. Radiogenic isotope ratios are correlated with major elements, indicating the effects of assimilation in all Period A lavas. In the two-stage assimilation and fractional crystallization model of Putirka et al. (2009) AFC-1 increases $^{87}Sr/^{86}Sr$ to generate primitive Craters of the Moon (COM) lavas, and these then assimilate shallower rhyolites (AFC-2) to produce the range of evolved COM compositions. Aside from the Trench Mortar Flat flow, the new Period A data conform to Magma Chamber Simulator (MCS) AFC-2 modeling in this study (model trends shown are offset from data for clarity), with primitive Period B-H samples as the parental magmas (samples G78K184 and H79K99; Putirka et al., 2009) and COM xenoliths (sample 78K181; Putirka et al., 2009), or central Eastern Snake River Plain rhyolites (sample PC-14a; Drew, 2013) as AFC-2 assimilants. MCS modeling steps show the proportions of the rhyolite assimilant in the magma required to produce the range of Period A compositions (up to 31%). Trench Mortar Flat compositions (violet symbols) follow a clearly divergent evolutionary path, indicating a lower magnitude of AFC-1, markedly different AFC-2 assimilation conditions, and/or a different assimilant from the other Period A flows.

and the commonly assigned $Fe^{2+}/Fe_{Total} = 0.85$ was used as the initial oxidation state for these runs and they were not buffered for oxygen (Heinonen et al., 2019; Luttinen & Furnes, 2000).

The MCS modeling results support a scenario in which all Period A flows except the Trench Mortar Flat are derived from the same parent magma generated by AFC-1, and subsequently underwent varying magnitudes of AFC-2 with Neogene rhyolites as wallrock assimilants. The Highway, Devil's Orchard, and Serrate Flows erupted following a circa 1,000 years hiatus after the last Period B eruptions (Kuntz, Spiker, et al., 1986), and their source magma may have spent a relatively longer amount of time cooling and exposed to shallow rhyolite before eruption, leading to their more evolved compositions. The modeling shows these to be plausible assimilation candidates, but coupled elemental and isotopic data for local rhyolites and xenoliths are limited in the literature, and more studies of these and other potential assimilants will be required to confirm this relationship.

A single, highly stratified magma body that fed seven of the eight Period A flows (except the Trench Mortar Flat flow) is consistent with the geochemical observations. However, given the abrupt change in heterogeneity and composition that occurred between the eruptions of the Serrate and Big Craters flows (Figure 4), initial storage in two physically separate but connected bodies (e.g., sills) would allow the two magma batches to evolve separately and avoid significant mixing, with magma for the first three flows stored in a shallower body more exposed to rhyolite and undergoing higher degrees of AFC (Figure 9). The most mafic samples recovered from the Devil's Orchard and Serrate flows have elemental and isotopic compositions that are essentially identical to samples from the Big Craters Flow that erupted after them (fourth) in the sequence (Figures 4 and 7c). These mafic samples may herald the initial appearance at the surface of the Big Craters magma from the second storage body, perhaps acting to trigger the earlier eruptions (Figure 9). Mafic recharge is considered a common eruption trigger to force evolved magmas in shallow storage to the surface (Cocker et al., 2022; Gansecki et al., 2019; Garcia et al., 1992; Hobden et al., 1999). The initial higher-silica magma appears to have been flushed out during the eruption of the Serrate Flow since the ensuing Big Craters and later mafic flows are much less heterogenous. The progressive evolution of the younger mafic flows may be due to the decreasing effects of AFC or due to decreasing contamination of the mafic magma by a diminishing residue of the previous high-silica magma in the conduit (Figure 9).

The Trench Mortar Flat Flow erupted in the Period A sequence between the time of the North Crater and Blue Dragon eruptions (Kuntz et al., 1992). Its several source vents are located on the Great Rift about 5–7 km to the south of those of the other Period A flows, and this geographic distinction is likely related to a separate magma source. Major elements for the Trench Mortar Flat Flow have subtle offsets from the trends shown by the other

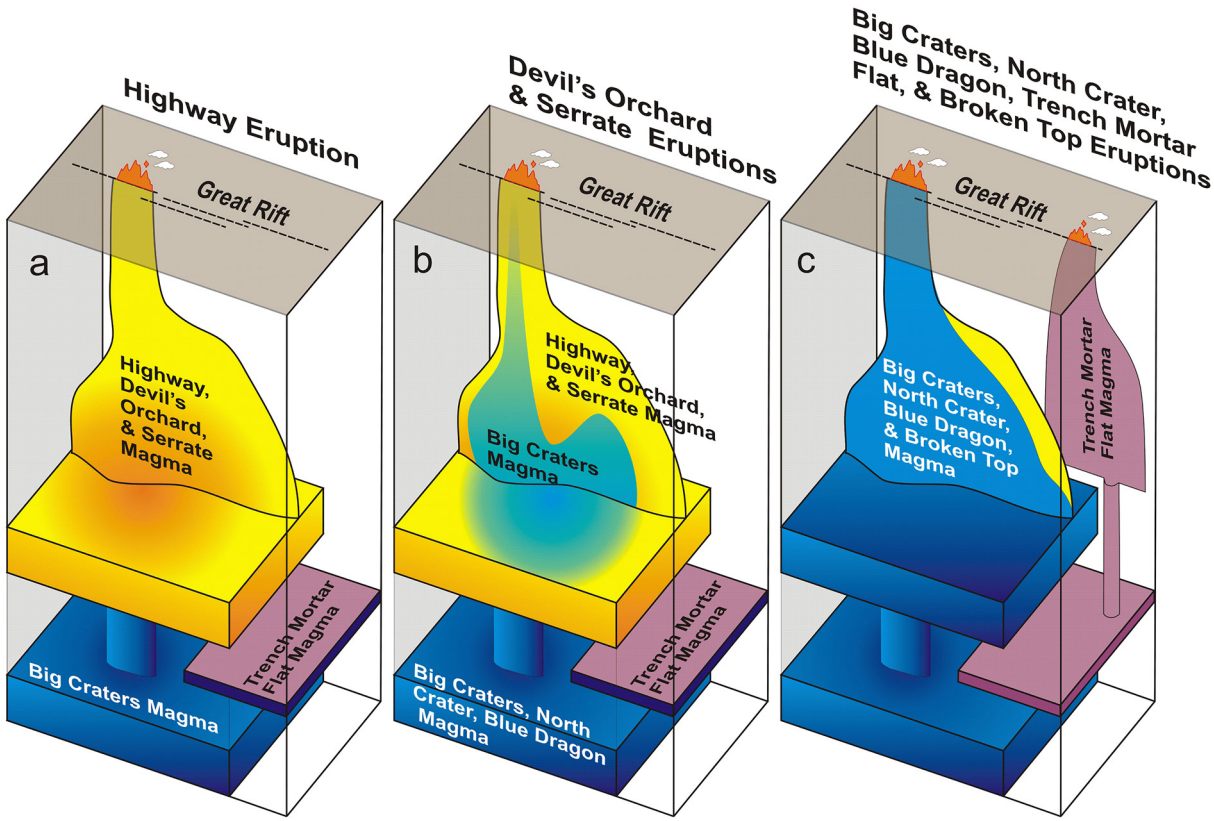

Figure 9. Diagrammatical model of the Period A eruptive sequence. The first three eruptions (Highway, Devil's Orchard, and Serrate flows) of Craters of the Moon Period A volcanism were likely derived from the same magma batch (yellow) and produced lavas with broad compositional variability that reflect poor homogenization and evolved compositions reflecting high extents of assimilation and fractional crystallization (AFC). The Big Craters, North Crater, Blue Dragon, and Broken Top flows became progressively more mafic and depleted, and represent either the lower portions of a single, stratified magma body or a separately stored batch (blue) that underwent less AFC. The Trench mortar Flat Flow erupted from fissures several km to the south of the others and has a distinct composition that requires a separate magma conduit (violet).

younger flows (Figure 2), it has distinctive Ni, REE, and Y concentrations and trace element ratios (Figures 5 and 6), and it has major element versus isotope correlations that deviate from the other flows (Figure 8). The Trench Mortar Flat parental magma was likely isolated from the source of the other seven flows and underwent a lower magnitude of AFC-1, then had different assimilation conditions and/or a different assimilant during AFC-2 (Figure 8).

The results of this study suggest that the Period A flows were fed by three discrete batches of magma that followed separate evolutionary paths. They provide insight into relatively short-term magmatic processes on the Great Rift fissure system, and also potentially into tectonic processes operating on the ESRP. The Period A eruptions in the 2,500 to 2,000 years BP period coincided with coeval eruptions of the Wapi and King's Bowl flows (2,270 and 2,222 years BP, respectively; Kuntz, Champion, et al., 1986) near the southern end of the Great Rift, possibly indicating a period of enhanced extension and magmatism on this prominent young ESRP fissure system.

5. Conclusions

The COM volcanic field is a prominent example of a long-lived, polygenetic fissure system and the locus of the most recent activity in the YSRP volcanic province. Period A was the last active eruptive period at COM and produced eight lava flows between about 2,500 and 2,000 years ago near the northern terminus of the Great Rift fissure zone. In this study, new high-precision major and trace element and Sr, Nd, and Pb isotope data for these flows reveal previously unrecognized temporal and compositional groups suggesting three separate source magma batches. The first three flows are derived from a heterogenous and highly evolved magma, and the four later flows are from a more mafic and homogenous magma. These two groups form coherent compositional

trends suggesting derivation from a common parent and related via different magnitudes of AFC, with Neogene rhyolite related to the passage of the Yellowstone hotspot as a plausible assimilant. The third compositional type was identified in the sixth flow in the Period A series, sourced from fissures about 5–7 km to the south of the other flows. It has characteristics that indicate a separate parental magma, AFC history, and conduit to the surface. Variable interflow compositions among these three Period A groups and compositional changes over the eruptive sequence are evidence of poorly homogenized and potentially stratified magma sources. These results provide valuable insights into processes that deliver magmas and control their compositions in polygenetic fissure volcanic systems.

Data Availability Statement

All geochemical data acquired in this study are provided in Table S1 and in an Earthchem.org database available at https://doi.org/10.26022/IEDA/112766.

Acknowledgments
This work was supported by internal research funds from the College of Charleston. The authors wish to acknowledge Todd Stefanic, Research Coordinator at Craters of the Moon National Monument for assistance with sample collection permits, and Michael McCurry for an insightful review that greatly improved this article.

References

Anders, M., & Sleep, N. (1992). Magmatism and extension: The thermal and mechanical effects of the Yellowstone hotspot. *Journal of Geophysical Research*, *97*(B11), 15379–15394. https://doi.org/10.1029/92JB01376

Bohrson, W., Spera, F., Heinonen, J., Brown, G., Scruggs, M., Adams, J., et al. (2020). Diagnosing open-system magmatic processes using the magma chamber simulator (MCS): Part I—Major elements and phase equilibria. *Contributions to Mineralogy and Petrology*, *175*(11), 104. https://doi.org/10.1007/s00410-020-01722-z

Braile, L., Smith, R., Ansorge, J., Baker, M., Sparlin, M., Prodehl, C., et al. (1982). The Yellowstone-Snake River Plain seismic profiling experiment: Crustal structure of the eastern Snake River Plain. *Journal of Geophysical Research*, *87*(B4), 2597–2609. https://doi.org/10.1029/JB087iB04p02597

Camp, V., Ross, M., Duncan, R., Jarboe, N., Coe, R., Hanan, B., & Johnson, J. (2013). The Steens basalt: Earliest lavas of the Columbia River basalt group. *The Columbia River Flood Basalt Province: Geological Society of America Special Paper*, *497*, 87–116. https://doi.org/10.1130/2013.2497(04)

Chadwick, J., Payne, S., Van Hove, T., & Rodgers, D. (2007). Contemporary tectonic motion of the eastern Snake River Plain: A campaign global positioning system study. *Tectonics*, *26*(6), TC6005. https://doi.org/10.1029/2005TC001914

Chadwick, J., Schwartz, M., Mclane, D., Collins, E., & Kamenov, G. (2019). Compositional heterogeneity of the 3.4 km^3 blue dragon flow, Craters of the Moon Volcanic Field, Idaho. *Journal of Volcanology and Geothermal Research*, *388*, 106690. https://doi.org/10.1016/j.jvolgeores.2019.106690

Christiansen, E., & McCurry, M. (2008). Contrasting origins of Cenozoic silicic volcanic rocks from the western Cordillera of the United States. *Bulletin of Volcanology*, *70*(3), 251–267. https://doi.org/10.1007/s00445-007-0138-1

Coble, M. A., & Mahood, G. A. (2012). Initial impingement of the Yellowstone plume located by widespread silicic volcanism contemporaneous with Columbia River flood basalts. *Geology*, *40*(7), 655–658. https://doi.org/10.1130/G32692.1

Cocker, K., Shane, P., Cronin, S., Stirling, C., & Reid, M. (2022). A history of andesite production via magma mixing and mingling revealed microscopically at Ngauruhoe volcano. *Geochemistry, Geophysics, Geosystems*, *23*(10), e2022GC010589. https://doi.org/10.1029/2022GC010589

DePaolo, D. (1981). Trace element and isotopic effects of combined wallrock assimilation and fractional crystallization. *Earth and Planetary Science Letters*, *53*(2), 189–202. https://doi.org/10.1016/0012-821X(81)90153-9

Drew, D. (2013). *An isotopic, trace element, and volatile investigation of large-volume rhyolite generation at the Picabo Volcanic Field of the Yellowstone hotspot track*. M.S. thesis, University of Oregon. Retrieved from http://hdl.handle.net/1794/17894

Foster, D., Mueller, P., Mogk, D., Wooden, J., & Vogl, J. (2006). Proterozoic evolution of the western margin of the Wyoming craton: Implications for the tectonic and magmatic evolution of the northern Rocky Mountains. *Canadian Journal of Earth Sciences*, *43*(10), 1601–1619. https://doi.org/10.1139/E06-052

Fouch, M. J. (2012). The Yellowstone hotspot: Plume or not? *Geology*, *40*(5), 479–480. https://doi.org/10.1130/focus052012.1

Gansecki, C., Lopaka Lee, R., Shea, T., Lundblad, S., Hon, K., & Parcheta, C., (2019). The tangled tale of Kīlauea's 2018 eruption as told by geochemical monitoring. *Science*, *366*, 6470. https://doi.org/10.1126/science.aaz0147

Ganske, R., & McCurry, M. (2006). Petrogenesis of A-type quaternary rhyolite and cogenetic mafic magmatic enclaves at east butte volcanic dome, eastern Snake River Plain, Idaho. In *Proceedings of the 2005 Great Rift science symposium* (pp. 49–55). Idaho Museum of Natural History Publication.

Garcia, M. O., Rhodes, J. M., Wolfe, E. W., & Ulrich, G. E. (1992). Petrology of lavas from episodes 2–47 of the Puu Oo eruption of Kilauea volcano, Hawaii: Evaluation of magmatic processes. *Bulletin of Volcanology*, *55*(1–2), 1–16. https://doi.org/10.1007/BF00301115

Greeley, R. (1982). The Snake River Plain, Idaho: Representative of a new category of volcanism. *Journal of Geophysical Research*, *87*(B4), 2705–2712. https://doi.org/10.1029/jb087ib04p02705

Gualda, G. A. R., Ghiorso, M. S., Lemons, R. V., & Carley, T. L. (2012). Rhyolite-MELTS: A modified calibration of MELTS optimized for silica-rich, fluid-bearing magmatic systems. *Journal of Petrology*, *53*(5), 875–890. https://doi.org/10.1093/petrology/egr080

Hanan, B., Shervais, J., & Vetter, S. (2008). Yellowstone plume–continental lithosphere interaction beneath the Snake River Plain. *Geology*, *36*(1), 51–54. https://doi.org/10.1130/g23935a.1

Heinonen, J. S., Bohrson, W. A., Spera, F. J., Brown, G., Scruggs, M., & Adams, J. (2020). Diagnosing open-system magmatic processes using the magma chamber simulator (MCS): Part II—Trace elements and isotopes. *Contributions to Mineralogy and Petrology*, *175*(11), 105. https://doi.org/10.1007/s00410-020-01718-9

Heinonen, J. S., Luttinen, A. V., Spera, F. J., & Bohrson, W. (2019). Deep open storage and shallow closed transport system for a continental flood basalt sequence revealed with Magma Chamber Simulator. *Contributions to Mineralogy and Petrology*, *174*(11), 87. https://doi.org/10.1007/s00410-019-1624-0

Hobden, B. J., Houghton, B. F., Davidson, J. P., & Weaver, S. D. (1999). Small and short-lived magma batches at composite volcanoes: Time windows at Tongariro volcano, New Zealand. *Journal of the Geological Society*, *156*(5), 865–868. https://doi.org/10.1144/gsjgs.156.5.0865

Hughes, S., McCurry, M., & Geist, D., (2002). Geochemical correlations and implications for the magmatic evolution of basalt flow groups at the Idaho National Engineering and Environmental Laboratory. *Geological Society of America Special Paper*, *353*, 151–173. https://doi.org/10.1130/0-8137-2353-1.151

Hughes, S., Nawotniak, S., Sears, D., Borg, C., Garry, W., Christiansen, E., et al. (2018). Phreatic explosions during basaltic fissure eruptions: Kings Bowl lava field, Snake River Plain, USA. *Journal of Volcanology and Geothermal Research*, *351*, 89–104. https://doi.org/10.1016/j.jvolgeores.2018.01.001

Hughes, S., Smith, R., Hackett, W., & Anderson, S. (1999). Mafic volcanism and environmental geology of the eastern Snake River Plain. In S. Hughes & G. Thackray (Eds.), *Guidebook to the geology of eastern Idaho: Pocatello, Idaho* (pp. 143–168). Idaho Museum of Natural History.

Irvine, N., & Baragar, W. (1971). A guide to the chemical classification of the common volcanic rocks. *Canadian Journal of Earth Sciences*, *8*(5), 523–548. https://doi.org/10.1139/e71-055

Jean, M., Hanan, B., & Shervais, J. (2014). Yellowstone hotspot-continental lithosphere interaction. *Earth and Planetary Science Letters*, *389*, 119–131. https://doi.org/10.1016/j.epsl.2013.12.012

Jordan, B. T., Grunder, A. L., Duncan, R., & Deino, A., (2004). Geochronology of age-progressive volcanism of the Oregon high lava plains: Implications for the plume interpretation of Yellowstone. *Journal of Geophysical Research*, *109*(B10), B10202. https://doi.org/10.1029/2003JB002776

Kamenov, G. D., Mueller, P., & Perfit, M. (2004). Optimization of mixed Pb-Tl solutions for high precision isotopic analyses by MC-ICP-MS. *Journal of Analytical Atomic Spectrometry*, *19*(9), 1262–1267. https://doi.org/10.1039/b403222e

Kamenov, G. D., Perfit, M. R., Mueller, P. A., & Jonasson, I. R. (2007). Controls on magmatism in an island arc environment: Study of lavas and sub-arc xenoliths from the Tabar-Lihir-Tanga-Feni island chain, Papua New Guinea. *Contributions to Mineralogy and Petrology*, *155*(5), 635–656. https://doi.org/10.1007/s00410-007-0262-0

Kuntz, M., Champion, D., Lefebvre, R., & Covington, H. (1988). *Geologic map of the Craters of the Moon, Kings Bowl, and Wapi lava fields, and the Great Rift volcanic zone, south-central Idaho*. U.S. Geological Survey Miscellaneous Investigations Series. Map I-1632. https://doi.org/10.3133/i1632

Kuntz, M., Champion, D., Spiker, E., & Lefebvre, R. (1986). Contrasting magma types and steady-state, volume-predictable, basaltic volcanism along the Great Rift, Idaho. *The Geological Society of America Bulletin*, *97*(5), 579–594. https://doi.org/10.1130/0016-7606(1986)97<579:CMTASV>2.0.CO;2

Kuntz, M., Champion, D., Spiker, E., Lefebvre, R., & McBroome, L. (1982). The Great Rift and the evolution of the Craters of the moon lava field, Idaho. In B. Bonnichsen & R. Breckenridge (Eds.), *Cenezoic geology of Idaho: Idaho bureau of mines and geology bull* (Vol. 26, pp. 423–437).

Kuntz, M., Covington, H., & Schorr, L. (1992). An overview of basaltic volcanism on the eastern Snake River Plain, Idaho. In P. Link, M. Kuntz, & L. Platt (Eds.), *Regional geology of eastern Idaho and western Wyoming* (pp. 227–268). Geological Society of America Memoir. https://doi.org/10.1130/MEM179-p227

Kuntz, M., Elsheimer, N., Espos, E., & Klock, P. (1985). Major-element analyses of latest pleistocene-holocene lava fields of the Snake River Plain, Idaho. *U.S. Geological Survey Open File Report*, *85–593*, 64. https://doi.org/10.3133/ofr85593

Kuntz, M., Lefebvre, R., Champion, D., & Skipp, B. (1989). *Geologic map of the inferno cone quadrangle, Butte county, Idaho* (Vol. 1632). U.S. Geological Survey Map GQ. https://doi.org/10.3133/gq1632

Kuntz, M., Skipp, B., Champion, D., Gans, P., Van Sistine, D., & Snyders, S. (2007). *Geologic map of the craters of the Moon 30' x 60' quadrangle, Idaho* (Vol. 2969). U.S. Geological Survey Scientific Investigations Map. https://doi.org/10.3133/sim2969

Kuntz, M., Spiker, E., Rubin, M., Champion, D., & Lefebvre, R. (1986). Radiocarbon studies of latest Pleistocene and Holocene lava flows of the Snake River Plain, Idaho: Data, lessons, interpretations. *Quaternary Research (Tokyo)*, *25*(2), 163–176. https://doi.org/10.1016/0033-5894(86)90054-2

Le Bas, M. J., Le Maitre, R. W., Streckeisen, A., & Zanettin, B. (1986). A chemical classification of volcanic rocks based on the total alkali-silica diagram. *Journal of Petrology*, *27*(3), 745–750. https://doi.org/10.1093/petrology/27.3.745

Leeman, W. (1982). Evolved and hybrid lavas of the Snake River Plain, Idaho. In B. Bonnichsen & R. Breckenridge (Eds.), *Cenezoic geology of Idaho* (Vol. 26, pp. 193–202). Idaho Bureau of Mines and Geology Bulleting.

Leeman, W., & Manton, W. (1971). Strontium isotopic compositions of basaltic lavas form the Snake River Plain, Idaho. *Earth and Planetary Science Letters*, *11*(1–5), 420–434. https://doi.org/10.1016/0012-821X(71)90204-4

Leeman, W., Menzies, M., Matty, D., & Embree, G. (1985). Strontium, neodymium, and lead isotopic compositions of deep crustal xenoliths from the Snake River Plain: Evidence for Archean basement. *Earth and Planetary Science Letters*, *75*(4), 354–368. https://doi.org/10.1016/0012-821X(85)90179-7

Leeman, W., Schutt, D., & Hughes, S. (2009). Thermal structure beneath the Snake River Plain: Implications for the Yellowstone hotspot. *Journal of Volcanology and Geothermal Research*, *188*(1–3), 57–67. https://doi.org/10.1016/j.jvolgeores.2009.01.034

Leeman, W., Vitaliano, C., & Prinz, M. (1976). Evolved lavas from the Snake River Plain: Craters of the moon national monument, Idaho. *Contributions to Mineralogy and Petrology*, *56*(1), 35–60. https://doi.org/10.1007/BF00375420

Le Maitre, R. W., Streckeisen, A., Zanettin, B., Le Bas, M. J., Bonin, B., & Bateman, P. (Eds.) (2002). *Igneous rocks: A classification and glossary of terms: Recommendations of the international union of geological Sciences subcommission on the systematics of igneous rocks* (2nd ed., p. 256). Cambridge University Press. https://doi.org/10.1017/CBO9780511535581

Luttinen, A., & Furnes, H. (2000). Flood basalts of Vestfjella: Jurassic magmatism across an Archaean-Proterozoic Lithospheric boundary in Dronning Maud Land, Antarctica. *Journal of Petrology*, *41*(8), 1271–1305. https://doi.org/10.1093/petrology/41.8.1271

Malde, H. (1991). Quaternary geology and structural history of the Snake River Plain, Idaho and Oregon. In R. Morrison (Ed.), *Quaternary nonglacial geology, Conterminous U.S.* (pp. 252–281). Geological Society of America, The geology of North America. https://doi.org/10.1130/DNAG-GNA-K2.251

McCurry, M., Hayden, K., Morse, L., & Mertzman, S. (2008). Genesis of post-hotspot, A-type rhyolite of the Eastern Snake River Plain volcanic field by extreme fractional crystallization of olivine tholeiite. *Bulletin of Volcanology*, *70*(3), 361–383. https://doi.org/10.1007/s00445-007-0143-4

McCurry, M., & Rogers, D. (2009). Mass transfer along the Yellowstone hotspot track I: Petrologic constraints on the volume of mantle-derived magma. *Journal of Volcanology and Geothermal Research*, *188*(1–3), 86–98. https://doi.org/10.1016/j.jvolgeores.2009.04.001

McQuarrie, N., & Rodgers, D. (1998). Subsidence of a volcanic basin by flexure and lower crustal flow: The eastern Snake River Plain, Idaho. *Tectonics*, *17*(2), 203–220. https://doi.org/10.1029/97TC03762

Menzies, M., Leeman, W., & Hawkesworth, C. (1984). Geochemical and isotopic evidence for the origin of continental flood basalts with particular reference to the Snake River Plain Idaho. USA. *Philosophical Transactions of the Royal Society of London. Series A, Mathematical and Physical Sciences*, *310*, 643–660. https://doi.org/10.1098/rsta.1984.0012

Nash, B., Perkins, M., Christensen, J., Lee, D., & Halliday, A. (2006). The Yellowstone hotspot in space and time: Nd and Hf isotopes in silicic magmas. *Earth and Planetary Science Letters*, *247*(1–2), 143–156. https://doi.org/10.1016/j.epsl.2006.04.030

Norman, M., & Mertzman, S. (1991). Petrogenesis of Challis volcanics from central and southwestern Idaho: Trace element and Pb isotopic evidence. *Journal of Geophysical Research*, *96*(B8), 13279–13293. https://doi.org/10.1029/91JB00285

Peng, X., & Humphreys, E. (1998). Crustal velocity structure across the eastern Snake River Plain and the Yellowstone swell. *Journal of Geophysical Research*, *103*(B4), 7171–7186. https://doi.org/10.1029/97JB03615

Pierce, K., & Morgan, L. (1992). The track of the Yellowstone hot spot: Volcanism, faulting, and uplift. In P. K. Link, M. A. Kuntz, & L. B. Platt (Eds.), *Regional geology of eastern Idaho and western Wyoming* (Vol. 179, pp. 1–53). Geological Society of America Memoir. https://doi.org/10.1130/MEM179-p1

Pierce, K., & Morgan, L. (2009). Is the track of the Yellowstone hotspot driven by a deep mantle plume? Review of volcanism, faulting, and uplift in light of new data. *Journal of Volcanology and Geothermal Research*, *188*(1–3), 1–25. https://doi.org/10.1016/j.jvolgeores.2009.07.009

Potter, K., Shervais, J., Christiansen, E., & Vetter, S. (2018). Evidence for cyclical fractional crystallization, recharge, and assimilation in basalts of the Kimama drill core, central Snake River Plain, Idaho: 5.5 million years of petrogenesis in a mid-crustal sill complex. *Frontiers of Earth Science*, *6*, 10. https://doi.org/10.3389/feart.2018.00010

Putirka, K., Kuntz, M., Unruh, D., & Vaid, N. (2009). Magma evolution and ascent at the Craters of the moon and neighboring volcanic fields, southern Idaho, USA: Implications for the evolution of polygenetic and monogenetic volcanic fields. *Journal of Petrology*, *50*(9), 1639–1665. https://doi.org/10.1093/petrology/egp045

Raczek, I., Stoll, B., Hofmann, A. W., & Jochum, K. P. (2001). High-precision trace element data for the USGS reference materials BCR-1, BCR-2, BHVO-1, BHVO-2, AGV-1, AGV-2, DTS-1, DTS-2, GSP-1 and GSP-2 by ID-TIMS and MIC-SSMS. *Geostandards and Geoanalytical Research*, *25*(1), 77–86. https://doi.org/10.1111/J.1751-908X.2001.TB00789.X

Rhodes, J., & Vollinger, M. (2004). Composition of basaltic lavas sampled by phase-2 of the Hawaii Scientific Drilling Project: Geochemical stratigraphy and magma types. *Geochemistry, Geophysics, Geosystems*, *5*(3), Q03G13. https://doi.org/10.1029/2002GC000434

Rodgers, D. W., Ore, H. T., Bobo, R. T., McQuarrie, N., & Zentner, N. (2002). Extension and subsidence of the eastern Snake River Plain, Idaho. In B. Bonnichsen, C. M. White, & M. McCurry (Eds.), *Tectonic and magmatic evolution of the Snake River Plain volcanic province: Idaho geological survey bulletin* (Vol. 30, pp. 121–155).

Shervais, J., & Hanan, B. (2008). Lithospheric topography, tilted plumes, and the track of the Snake River-Yellowstone hot spot. *Tectonics*, *27*(5), TC5004. https://doi.org/10.1029/2007TC002181

Shervais, J., Vetter, S., & Hanan, B. (2006). Layered mafic sill complex beneath the eastern Snake River Plain: Evidence from cyclic geochemical variations in basalt. *Geology*, *34*(5), 365–368. https://doi.org/10.1130/G22226.1

Smith, R., Jordan, M., Steinberger, B., Puskas, C., Farrell, J., Waite, G., et al. (2009). Geodynamics of the Yellowstone hotspot and mantle plume: Seismic and GPS imaging, kinematics, and mantle flow. *Journal of Volcanology and Geothermal Research*, *188*(1–3), 26–56. https://doi.org/10.1016/j.jvolgeores.2009.08.020

Stearns, H. (1928). *Craters of the moon national monument, Idaho* (Vol. 13, p. 57). Idaho Bureau of Mines and Geology Bulletin. Retrieved from http://www.npshistory.com/publications/geology/state/id/1928-13/sec1.htm

Stout, M., & Nicholls, J. (1977). Mineralogy and petrology of quaternary lava from the Snake River Plain, Idaho. *Canadian Journal of Earth Sciences*, *14*(9), 2140–2156. https://doi.org/10.1139/e77-181

Stout, M., Nicholls, J., & Kuntz, M. (1989). *Fractionation and contamination processes, Craters of the moon lava field, Idaho, 2000-2500 years B.P* (Vol. 131, p. 259). Bureau of Mines and Mineral Resources Bulletin. Retrieved from https://statesurveys.americangeosciences.org/vufind/Record/1991004530

Stout, M., Nicholls, J., & Kuntz, M. (1994). Petrological and mineralogical variations in 2,500–2,000 yr B.P. lava flows, Craters of the moon lava field, Idaho. *Journal of Petrology*, *35*(6), 1681–1715. https://doi.org/10.1093/petrology/35.6.1681

Sun, S. S., & McDonough, W. F. (1989). Chemical and isotopic systematics of oceanic basalts; implications for mantle composition and processes. In A. D. & M. J. Norry (Eds.), *Magmatism in the ocean basins. Saunders* (Vol. 42, pp. 313–345). Geological Society of London. https://doi.org/10.4236/ajcm.2017.73024

Whitehead, R. (1992). *Geohydrologic framework of the Snake River Plain aquifer system, Idaho and eastern Oregon* (No. (1408-B), p. 32). US Government Printing Office.